

横向激励多大气压 CO₂ 激光器卢越^{1,2}, 朱子任^{1,2}, 白进周^{1,2}, 叶静涵^{1,2}, 谭荣清¹, 郑义军^{1*}, 李业军^{3**}¹中国科学院空天信息创新研究院, 北京 100094;²中国科学院大学电子电气与通信工程学院, 北京 100049;³中国原子能科学研究院, 北京 102413

摘要 典型的可调谐横向激励大气压[TE(A)] CO₂ 激光器输出激光的脉冲宽度为 100~300 ns, 并伴有 3~10 μs 的脉冲“拖尾”, 在 9~11 μm 范围内输出约 100 条分立谱线。针对窄脉冲和连续调谐 CO₂ 激光器的应用需求, 开展了多大气压 CO₂ 激光器的研究。采用高压脉冲调制电源, 结合高气压脉宽压缩和光栅选线技术, 实现连续调谐红外激光输出, 脉冲宽度为 30~50 ns。当工作电压为 72 kV、气压为 7.07×10^5 Pa 时, 输出激光脉冲的能量为 590 mJ, 脉冲宽度为 35.7 ns, 并在 10R(32)至 10R(26)谱线之间实现连续调谐输出。

关键词 激光器; CO₂ 激光器; 多大气压; 连续调谐; 脉宽压缩

中图分类号 TN248.2

文献标志码 A

DOI: 10.3788/CJL202249.2301008

1 引言

脉冲 CO₂ 激光器具有高峰值功率、谱线调谐等特性, 在激光光谱学^[1-4]、激光化学^[5]、激光医疗^[6]、激光制造^[7-9] 和军事应用^[10] 等方面有巨大的潜力。横向激励大气压[TE(A)]CO₂ 激光器工作气压在 1 atm(约 1.01×10^5 Pa) 附近, 其输出的激光脉冲宽度通常在百纳秒量级, 且有若干微秒的脉冲“拖尾”, 如需实现远距离探测^[11], 则需要脉冲宽度更窄的激光。为获得纳秒量级的窄脉冲, 目前通常采用锁模^[12]、调 Q^[13] 以及等离子体开关^[14] 等方式。相比之下, 提高工作气体压强的方法具有独特的优势, 可以同时实现脉冲宽度的压缩和输出谱线的连续调谐。在连续调谐 CO₂ 激光器中, CO₂ 受激辐射产生的光子可以精确对准特定波长进行拉曼散射, 获得远红外乃至太赫兹激光源, 用于分离同位素等高精尖领域^[15-16]。

2015 年 von Bergmann 等^[17] 通过 HP10 激光系统在 10 atm 条件下实现激光输出, 脉宽为 60~150 ns, 脉冲能量为 250 mJ。本文采用高压脉冲调制电源, 在工作电压为 72 kV、气压为 7 atm 的条件下, 获得最小脉宽为 35.7 ns 的激光输出, 对应最大脉冲能量为 590 mJ, 呈现无“拖尾”的窄脉冲时域波形, 峰值功率可达 16 MW, 并在 10R(32)至 10R(26)谱线之间实现了连续调谐输出。

2 实验装置

图 1 为多大气压 CO₂ 激光器实验装置示意图。该激光器主要由能量注入单元、激光器腔体主放电单元和谐振腔单元三部分构成。

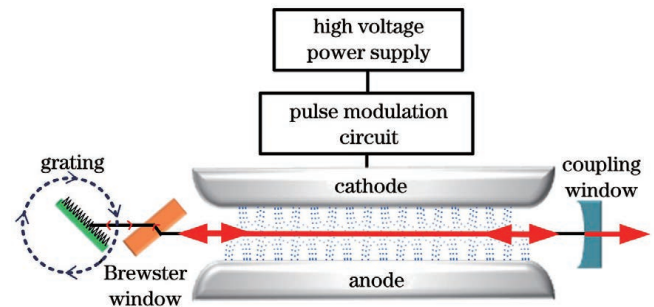


图 1 实验装置示意图

Fig. 1 Schematic diagram of experimental setup

工作时激光器腔体内充入不同气压的工作气体。高压电源输出的直流电压经脉冲调制电路后为腔体内主放电注入能量, 气体分子在放电时因能级跃迁释放出光子, 并在谐振腔内振荡, 直至增益大于损耗时输出激光。通过控制端驱动电机带动光栅旋转不同的角度, 可以选择输出不同波长的谱线。

由高压直流电源(≤ 32 kV)和脉冲调制电路构成能量注入单元, 作为该激光器的泵浦源。其中, 高压直流电源(24 kV)经过脉冲调制电路后耦合输出 72 kV 直流高压, 注入能量为 19.88 J, 注入能量密度

收稿日期: 2022-01-25; 修回日期: 2022-03-04; 录用日期: 2022-04-14

基金项目: 稳定基础科研计划资助(BJ19001810)

通信作者: *yjzheng@mail.ie.ac.cn; **iamliyejun@163.com

为 47.33 J/(L · atm)。

为避免腔体内外压差引起形变,激光器腔体采用高强度碳钢,平均厚度 ≥ 20 mm,接口处采用牙角为 60° 的干密封布氏锥螺纹(即美国标准锥管螺纹)连接,并匹配不锈钢针阀用于更换工作气体。在密封方面,该激光器采用内嵌型加厚光学窗口设计,有效避免内外压力差导致的窗口破裂,缓解窗口变形引起的光斑畸变。实验时在激光器腔体内充入气体混合物,CO₂、N₂ 和 He 的体积比为 V_{CO₂} : V_{N₂} : V_{He} = 2 : 1 : 16。放电过程主要分为预电离和主放电两部分。预电离系统由位于主电极侧面的两排钨针构成,其耦合电路与主放电回路并共用一个电源,预电离放电在主放电前数十纳秒开始,辐射紫外光使放电区气体电离,使电极间获得一定的初始电子浓度,为大面积均匀场放电创造条件。预电离效果消失后,主放电继续进行,直至储能电容能量泄放完成。预电离能够增加放电稳定性。主放电在两电极之间进行,电极采用 Chang 氏铝电极,增益体积为 10 mm × 10 mm × 600 mm。

谐振腔采用平凹腔,腔长为 1 m,由部分反射的锩镜作为输出耦合窗口(反射率 R = 36%)和工作在利特罗角的衍射光栅(光栅常数 1/150 mm)组成,其中输出镜曲率半径为 4 m。输出镜装在设计有内嵌型光学窗口的腔体端板一侧,光栅装在激光器腔体外侧,由电机驱动光栅旋转,实现不同波长的调谐输出。该谐振腔为半外腔,因此在靠近光栅一侧的腔体端板处装有布儒斯特窗口。该布儒斯特窗口偏折角度为 67°,材质为硒化锌,既可用于密封激光器腔体,形成光束通路,又可以减小损耗,便于研究激光的输出特性。

3 结果与分析

实验中采用 Coherent-J100MB 探头和 Coherent EPM2000 表头探测脉冲能量;Opt. Eng16A 光谱仪用于验证谱线波长;滨松 B749 光子牵引探测器和 Tektronix DPO4104B 数字荧光示波器用于记录脉冲波形。

针对多大气压 CO₂ 激光器,利用六温度多频动力学模型^[18] 计算 CO₂ 分子运动过程,并采用四阶 Runge-Kutta 法进行数值分析,可以通过理论计算得

出脉冲宽度和能量,通过数值计算得出 CO₂ 分子输出频谱和增益谱分布。

在激光产生过程中,第 *i* 个频率成分的输出功率^[19] 如下:

$$P_i = -\frac{\pi}{8} D_M^2 F \ln(R T_r) \frac{1 - R - K_M}{1 - R T_r} h c \nu_i Q_i, \quad (1)$$

式中: D_M 为输出镜直径; F 为填充因子; R 为输出镜反射率; T_r 和 K_M 为输出耦合镜除透射外的吸收等损耗,通常 $T_r = 1, K_M = 0$; h 为普朗克常量; c 为光速; ν_i 为第 *i* 个频率成分激光的频率; Q_i 为第 *i* 个频率成分的光子数密度。

对应的第 *i* 个频率成分的脉冲能量为

$$E_i = \int_i P_i(t) dt. \quad (2)$$

对上述等式进行数值积分计算时可简化为

$$E_i = \sum_m dP_i(md), \quad (3)$$

式中: d 为步长。

对上述所有频率成分的输出功率求和即可得出输出激光的脉冲波形。根据脉冲波形可计算出脉冲宽度和峰值功率。输出的激光脉冲能量 E_i 与频率 ν_i 的函数曲线即为输出频谱。

对于 CO₂ 激光器,谐振腔内工作气体在某一频率处的增益系数表达式^[19] 为

$$G = \sigma_{00^0_1}(\nu_i) N_{00^0_1} - \sigma_{10^0_0}(\nu_i) N_{10^0_0}, \quad (4)$$

式中: $\sigma_{00^0_1}$ 和 $\sigma_{10^0_0}$ 分别为 CO₂ 上下振动能级受激辐射截面; $N_{00^0_1}$ 和 $N_{10^0_0}$ 分别为激光上下振动能级的粒子数密度。

对六温度多频动力学模型进行数值计算,根据求得各振动温度和气体温度瞬时解可以计算出受激辐射截面值,代入式(4),即可得到信号增益随频率分布的增益谱曲线。

图 2(a) 是脉冲放电电路图,其中充电电阻 $R_1 = 15 \text{ k}\Omega$,接地电阻 $R_2 = 5 \text{ k}\Omega$,储能电容 $C_0 = 23 \text{ nF}$,接地电容 $C_1 = 1 \text{ nF}$, C_2, C_3, C_4 分别为三级耦合电容, $C_2 = 140 \text{ pF}$, $C_3 = 160 \text{ pF}$, $C_4 = 200 \text{ pF}$,预电离电容 $C_5 = 1 \text{ nF}$,峰化电容 $C_6 = 1 \text{ nF}$,接地电感 $L = 2 \text{ }\mu\text{H}$,

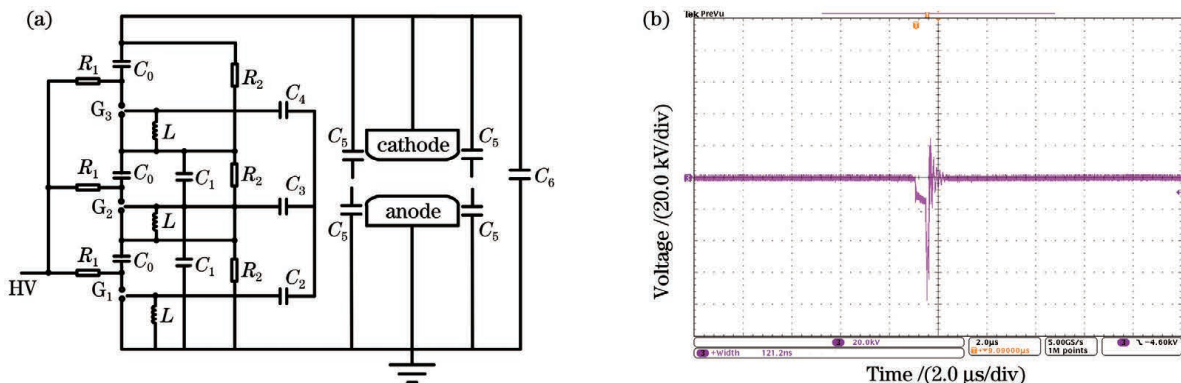


图 2 脉冲放电电路图与波形图。(a) 电路图; (b) 放电波形图

Fig. 2 Pulse discharge circuit diagram and discharge waveform. (a) Circuit diagram; (b) discharge waveform

G_1 、 G_2 、 G_3 为三个球隙开关,球隙间距均为 8 mm。高压电源给三组储能电容充电后再触发串联放电,实现三倍压的脉冲输出。

图 2(b) 曲线是放电电压波形。放电电压超过 70 kV,脉宽为纳秒量级。上述电路中均采用高频低损耗的元器件,且其分布电感和主放电回路的阻抗较小,因此储能电容能量泄放很快,能够实现窄脉冲输出。

3.1 脉冲输出特性

气体工作气压与 CO_2 分子上能级寿命之间的关系为^[20]

$$P\tau = C, \quad (5)$$

式中: P 为气体工作气压; τ 为 CO_2 分子上能级寿命; C 为常数。

气体工作气压与 CO_2 分子上能级寿命成反比,气压升高,上能级寿命缩短。在激光产生过程中, CO_2 分子自由振荡产生振转能级跃迁,处于激发状态的粒子由于上能级寿命缩短,能在较短的时间内跃迁至下能级,此时受激辐射产生的激光脉冲脉宽被压缩。

计算出输出脉冲波形后,由波形可计算出不同大气压下输出脉冲的脉宽值。图 3 是激光器输出 10P(20) 脉冲的脉宽随气压变化图。理论计算时增益体积与实验保持中一致,为 10 mm × 10 mm × 600 mm,输出镜的反射率 $R = 36\%$,气体混合物的体积比为 $V_{\text{CO}_2} : V_{\text{N}_2} : V_{\text{He}} = 2 : 1 : 16$ 。可以看出,脉冲

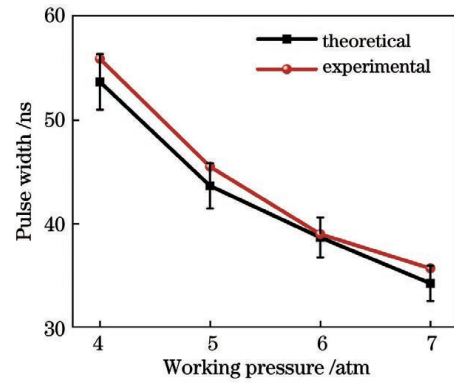


图 3 多大气压下输出脉宽理论与实验值

Fig. 3 Theoretical and experimental values of output pulse width in multi-atmospheric-pressure CO_2 laser

宽度随着气压升高逐渐变小。在 4~7 atm 范围内,实验值与理论值吻合度较好,误差小于 5%。这些误差可能是由气体压强测量误差引起的。

假设气体温度为 300 K,仅考虑耦合镜吸收损耗,其余实验条件均处于理想状态下,建立理论模型。图 4 比较了多大气压下的理论计算与实验输出脉冲波形。由图 3 和图 4 可以看出,脉冲宽度的测量值比理论值偏大,这是因为在实验过程中,气体温度会随着放电时间延长而逐渐升高,同时存在其他未考虑到的实验损耗等因素,理论计算得到的脉冲波形的上升沿和下降沿斜率更大,相同注入下的脉冲宽度更小。

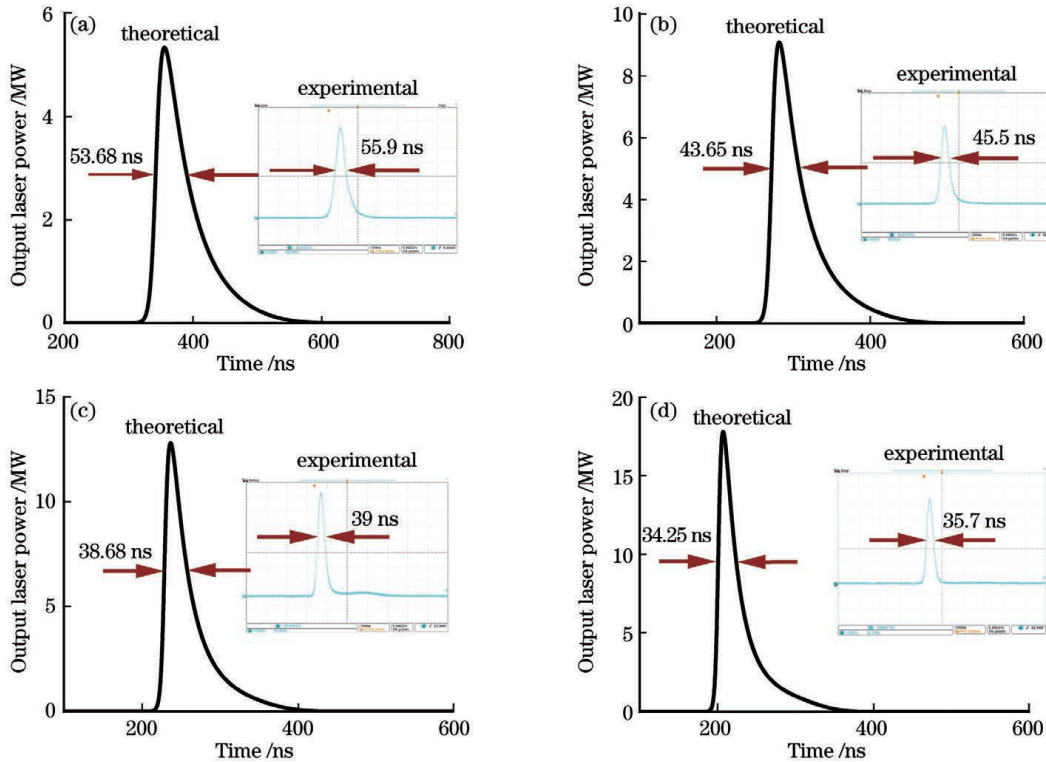


图 4 多大气压下的理论计算与实验输出脉冲波形图。(a) 4 atm;(b) 5 atm;(c) 6 atm;(d) 7 atm

Fig. 4 Theoretical and experimental output pulse waveforms in multi-atmospheric-pressure CO_2 laser. (a) 4 atm; (b) 5 atm; (c) 6 atm; (d) 7 atm

如图 4(d) 所示,在 7 atm 条件下,10P(20) 脉冲无明显拖尾,脉宽为 35.7 ns,峰值功率为 16 MW。相比

于 TE(A) CO_2 激光器(脉宽 100~300 ns,峰值功率 10 MW),脉宽压缩约 85%,峰值功率提高 60%。

基于理论计算得出的数值结果可以充分验证实验方案的可行性,而实验结果也与理论计算得出的脉宽随气压升高不断压缩、峰值功率有所提高的趋势吻合。

图 5 为多大气压下脉冲能量的理论值与实验值的对比图。可以看出,脉冲能量随着气压的升高而增加。这是由于当气压升高时,所需工作电压升高,能量注入增大。在 4 ~ 7 atm 范围内,测量值与理论值吻合度较好,误差小于 5%。

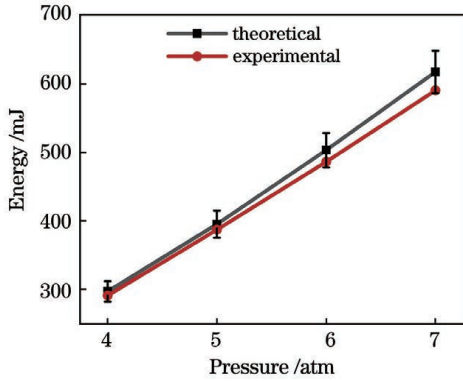


图 5 多大气压下输出能量理论与实验值

Fig. 5 Theoretical and experimental values of output energy in multi-atmospheric-pressure CO₂ laser

图 6 为工作气压分别为 2 atm 和 7 atm 时输出能量谱分布图。从图 6 可以看出,气压升高,谱带(9R、9P、10R、10P)输出谱线的线宽变窄。当气压为 7 atm 时,原来处于谱带边缘的弱线处无能量输出,这是由于:在增益强的谱线处线宽展宽,增益大于损耗,输出谱线波长范围被拓宽;而在增益弱的谱线处,线宽展宽后,增益小于损耗,谐振腔内无振荡输出。

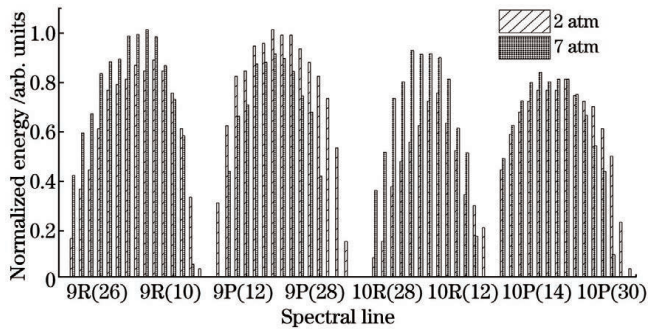


图 6 不同气压下输出能量谱分布图

Fig. 6 Output energy distributions under different pressures

3.2 连续调谐

定义增益谱的调制度为

$$M = \frac{G_{\max} - G_{\min}}{G_{\max} + G_{\min}}, \quad (6)$$

式中: M 为调制度; G_{\max} 为谱线中心增益; G_{\min} 为两中心谱线之间的最小增益。

根据式(4)可以计算归一化增益谱分布。为方便讨论,选取 10P 支、10R 支得到理论计算结果,如图 7 所示。随着气压的升高,CO₂ 分子的谱线由分立状态逐渐变成连续状态,增益谱的调制度逐渐减小,谱线重

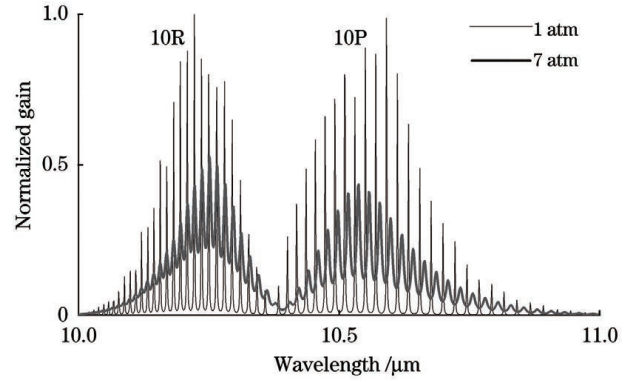


图 7 CO₂ 分子增益谱分布

Fig. 7 Normalized gain spectrum distribution of CO₂ molecules

叠部分逐渐增加。在 7 atm 条件下,P 支的调制度约为 35%,R 支的调制度约为 15%,R 支谱线振转跃迁的间隔平均为 0.012 μm,小于 P 支谱线振转跃迁的平均间隔 0.021 μm。可以得出,在相同条件下,R 支比 P 支调制度小,重叠效果更好,谱线也更加平滑。

图 8 是以 10R 支为例,基于式(3)绘制的频谱特性分布图。通过 PC 控制端转动电机,带动光栅转动一定角度。根据光栅方程^[21]:

$$2d \sin \theta = k\lambda, \quad (7)$$

计算得出每转动 14",光栅波长变化 $5.86 \times 10^{-4} \mu\text{m}$ 。图 8 中散点为在 7 atm 时实验测得的输出脉冲能量,曲线是理论计算值。从图 8 可知,在波长 10.172 ~ 10.212 μm 之间可连续测得激光脉冲输出能量,在 10R(26)、10R(28)、10R(30)、10R(32)处获得较高的输出能量,在两线间能量下降平均值约为 70%,并且可从光谱仪中观测到混线现象,临近该波长处的两条谱线均可以振荡输出。当光栅转动到弱线对应的角度时,随着增益逐渐减小,两中心谱线间能量下降也逐渐显著。因为理论计算时只考虑了激光器腔体内增益损耗和输出耦合镜透射的吸收损耗,并未充分考虑其他损耗,并且理论计算过程中假设工作气体温度为 300 K 不变,但是实际实验中工作气体在高压下电离会释放热能,气体温度逐渐上升,所以实验测得的输出能量值略低于理论计算值。在波长小于 10.165 μm

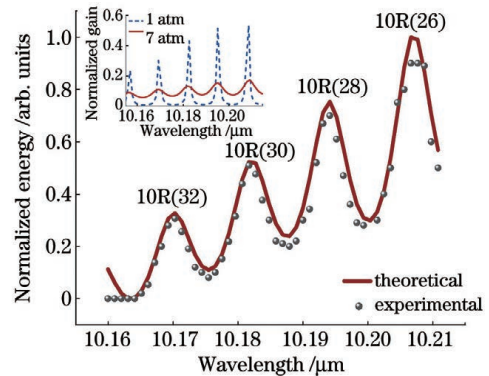


图 8 输出频谱特性理论计算与实验对比图

Fig. 8 Theoretical and experimental graphs of output spectrum characteristics

时,由于增益小于损耗,实验未能测得能量,与理论计算结果略有差异。总体来说,曲线较好地拟合了实验值,同时实验结果也印证了理论上气压升高引起的相邻谱线的增益重叠,从而实现连续调谐。由此可认为,本文提出的多大气压 CO₂ 激光器在气压升高至 7 atm 时可实现连续调谐输出。但是由于气压升高,谱线展宽,弱线处增益下降,因此实验测得的 10R 支谱带范围有所缩减。

4 结 论

本文研究了一种多大气压脉冲 CO₂ 激光器,在 9.2~10.8 μm 范围内的 4 个分支(9R、9P、10R、10P)上,用光栅实现了连续调谐输出。von Bergmann 等^[17]在 10 atm,气体混合物的比例为 V_{CO₂} : V_{N₂} : V_{He} = 1 : 1 : 25 的实验条件下,实现了脉宽为 60~150 ns、能量为 250 mJ 的激光输出;本文采用反射率 R = 36% 的锗镜作为输出镜,气体混合物的比例为 V_{CO₂} : V_{N₂} : V_{He} = 2 : 1 : 16,当工作气压为 7 atm、放电电压为 72 kV、注入能量为 19.88 J 时,在 10P(20)处输出的激光脉冲的能量为 590 mJ,脉宽为 35.7 ns,峰值功率为 16 MW。在进行参量优化后,本文实验相较于 von Bergmann 等^[17]的实验,使用相同的增益体积,在更低的气压下,脉宽压缩近 50%,能量提升两倍以上,峰值功率提高四倍,输出谱线范围从 9R(32)至 10P(30)共计 50 条[von Bergmann 等^[17]实验获得从 9R(28)至 10P(26)输出谱线 39 条]。本文的研究为多大气压 CO₂ 激光器实现脉宽压缩和连续调谐提供了实验依据。

参 考 文 献

- [1] Miller J L. The high-pressure absorption spectra of the CO₂ 10.6- and 9.4-μm laser bands[J]. *Journal of Applied Physics*, 1978, 49(6): 3076-3083.
- [2] Geiko P P, Tikhomirov A. Remote measurement of chemical warfare agents by differential absorption CO₂ lidar[J]. *Optical Memory and Neural Networks*, 2011, 20(1): 71-75.
- [3] Dumitras D C, Banita S, Bratu A M, et al. Ultrasensitive CO₂ laser photoacoustic system[J]. *Infrared Physics & Technology*, 2010, 53(5): 308-314.
- [4] Mrázek J, Aubrecht J, Todorov F, et al. CO₂ laser-assisted preparation of transparent Eu₂Ti₂O₇ thin films[J]. *Ceramics International*, 2018, 44(8): 9479-9483.
- [5] Tan C, Zhao L J, Chen M J, et al. Combined studies of surface evolution and crack healing for the suppression of negative factors during CO₂ laser repairing of fused silica[J]. *Chinese Optics Letters*, 2021, 19(4): 041402.
- [6] Holder D, Leis A, Buser M, et al. High-quality net shape geometries from additively manufactured parts using closed-loop controlled ablation with ultrashort laser pulses[J]. *Advanced Optical Technologies*, 2020, 9(1/2): 101-110.
- [7] 陈亮, 刘晓东, 刘静, 等. 飞秒激光在石英玻璃表面刻蚀微槽的研究[J]. *光学学报*, 2020, 40(23): 2314001.
Chen L, Liu X D, Liu J, et al. Microgroove etching with femtosecond laser on quartz glass surfaces[J]. *Acta Optica Sinica*, 2020, 40(23): 2314001.
- [8] Wang S Y, Ma Y W, Li X Y, et al. Highly sensitive torsion sensor based on triangular-prism-shaped long-period fiber gratings[J]. *Chinese Optics Letters*, 2021, 19(4): 041202.
- [9] 贾卓楠, 张婷婷, 栗正华, 等. 基于 CO₂ 激光加工的法布里-珀罗光学微腔阵列的制备[J]. *激光与光电子学进展*, 2020, 57(23): 231404.
Jia Z N, Zhang T T, Li Z H, et al. Fabrication of Fabry-Pérot optical microcavity array based on CO₂ laser processing[J]. *Laser & Optoelectronics Progress*, 2020, 57(23): 231404.
- [10] Nafisah S, Sumatera I T, Tukiran Z, et al. Laser technology applications in critical sectors: military and medical[J]. *Journal of Electronic Voltage and Application*, 2021, 2(1): 38-48.
- [11] 李道京, 周凯, 崔岸婧, 等. 多通道逆合成孔径激光雷达成像探测技术和实验研究[J]. *激光与光电子学进展*, 2021, 58(18): 1811017.
Li D J, Zhou K, Cui A J, et al. Multi-channel inverse synthetic aperture lidar imaging detection technology and experimental research[J]. *Laser & Optoelectronics Progress*, 2021, 58(18): 1811017.
- [12] 石宇航, 程昭晨, 彭志刚, 等. 21 MHz~100 kHz 重复频率亚皮秒 NALM 锁模光纤激光器[J]. *中国激光*, 2021, 48(5): 0501013.
Shi Y H, Cheng Z C, Peng Z G, et al. Sub-picosecond NALM mode-locked fiber laser with 21 MHz~100 kHz repetition rate[J]. *Chinese Journal of Lasers*, 2021, 48(5): 0501013.
- [13] Yuzaile Y R, Awang N A, Zalkepli N U H H, et al. Pulse compression in Q-switched fiber laser by using platinum as saturable absorber[J]. *Optik*, 2019, 179: 977-985.
- [14] 李红霞, 楼祺洪, 董景星, 等. 准分子激光等离子体开关控制脉宽研究[J]. *强激光与粒子束*, 2006, 18(7): 1090-1094.
Li H X, Lou Q H, Dong J X, et al. Excimer laser plasma switch controlling laser pulse duration[J]. *High Power Laser and Particle Beams*, 2006, 18(7): 1090-1094.
- [15] Snyder R. A proliferation assessment of third generation laser uranium enrichment technology[J]. *Science & Global Security*, 2016, 24(2): 68-91.
- [16] Saini V K, Talwar S, Subrahmanyam V V V, et al. Laser assisted isotope separation of lithium by two-step photoionization using time of flight mass-spectrometer[J]. *Optics & Laser Technology*, 2019, 111: 754-761.
- [17] von Bergmann H, Morkel F. Continuously wavelength tunable high pressure CO₂ lasers[J]. *Proceedings of SPIE*, 2015, 9255: 92551Y.
- [18] 丁长林, 万重怡. 脉冲 CO₂ 激光器的多频动力学模型[J]. *物理学报*, 2006, 55(3): 1165-1170.
Ding C L, Wan C Y. Multifrequency dynamical model of pulsed CO₂ lasers[J]. *Acta Physica Sinica*, 2006, 55(3): 1165-1170.
- [19] Smith K, Thomson R M. Computer modeling of gas lasers[M]. New York: Springer, 1978.
- [20] 楼祺洪. 脉冲放电气体激光器[M]. 北京: 科学出版社, 1993: 47-48.
Lou Q H. The pulse discharge gas laser[M]. Beijing: Science Press, 1993: 47-48.
- [21] 郁道银, 谈恒英. 工程光学[M]. 4 版. 北京: 机械工业出版社, 2014.
Yu D Y, Tan H Y. Engineering optics[M]. 4th ed. Beijing: China Machine Press, 2014.

Transversely Excited Multi-Atmospheric-Pressure CO₂ Laser

Lu Yue^{1,2}, Zhu Ziren^{1,2}, Bai Jinzhou^{1,2}, Ye Jinghan^{1,2}, Tan Rongqing¹, Zheng Yijun^{1*},
Li Yejun^{3**}

¹ Aerospace Information Research Institute, Chinese Academy of Sciences, Beijing 100094, China;

² School of Electronic, Electrical and Communication Engineering, University of Chinese Academy of Sciences, Beijing 100049, China;

³ China Institute of Atomic Energy, Beijing 102413, China

Abstract

Objective High peak power and continuous tuning are main characteristics of transversely excited atmospheric-pressure [TE(A)] CO₂ lasers which have great potential applications in laser spectroscopy, laser chemistry, laser medicine, laser manufacturing, military and so on. Unlike those working at a pressure around 1 atm, tailing phenomenon is mostly eliminated in multi-atmospheric-pressure CO₂ lasers and the pulse width is compressed from hundreds nanoseconds to tens nanoseconds level, so that the total interactive efficiency of the abovementioned applications is further improved. Compared with other pulse width compressing techniques such as mode-locking, Q-switching, plasma switching, etc., another advantage of multi-atmospheric-pressure CO₂ laser is the integration of narrow pulse width and continuous tuning. Such a laser can achieve accurate output of arbitrary wavelength in the 9–11 μm range. A typical application is proved to realize stimulated Raman scattering and excite isotope molecules, which may be an alternative high efficiency solution of present huge separation facilities.

Methods The theory consists of the continuously tunable theory and multifrequency dynamic model. The continuously tunable theory means that as the working pressure increases, the discrete spectral lines are gradually broadened until they overlaps each other, so the output becomes continuously tunable. The multifrequency dynamic model can describe the progress of pulsed CO₂ laser at high pressure. In this model, changing the electricity, gas and optical parameters can result in different output laser pulse waveforms, which can be further used to analyze the output characteristics such as energy, pulse width, power and wavelength. In experiment, a multi-atmospheric-pressure pulsed CO₂ laser was set up. The laser mainly consisted of the energy injection unit, the main discharge unit and the resonant cavity. A high voltage DC power supply (≤ 32 kV) and a triple Marx circuit were used for power supply and pulse modulation in the energy injection circuit. The pre-ionization structures and main discharge electrodes were arranged inside the chamber. The chamber was filled with gas mixture of carbon dioxide, nitrogen and helium. The resonant cavity adopted a plane-concave cavity type, which contained an output coupling window (the coupling mirror made of Ge) and a diffraction grating. The grating was driven by a server motor working at the Littrow angle (with the grating constant of 1/150 mm) to realize a tunable output. By substituting the optimal parameters obtained from the experiment into the theoretical model and analyzing the output pulse characteristics, it is found that the theoretical results are consistent with the experimental values. Thus the experiment is proven reasonable and correct.

Results and Discussions The output properties of transversely excited multi-atmospheric-pressure CO₂ lasers are studied in this paper. Under a working pressure of 7 atm, an output with 590 mJ pulse energy and corresponding 35.7 ns pulse width is obtained. It has been reported in 2015 that von Bergmann *et al.* generated short pulses around 250 mJ and 60–150 ns under the pressure of 1–10 atm. In comparison with former studies, we raised the pulse energy record by nearly 100% and compressed the minimum pulse width record by nearly 50%. Furthermore, a continuously tunable property was observed at a lower pressure of 7 atm. More than 30 mJ average output was detected every 5.86×10^{-4} μm from line 10R(32) to line 10R(26). However, the band range measured in experiment was reduced since the loss was bigger than the gain at the edge of four bands as the working pressure rose (Fig. 6). Meanwhile, the modulation degree of the R band is smaller than that of the P band, leading to the smoother output distribution of the R band (Fig. 7). The whole data acquired under lower pressure perform obvious continuous tuning properties and growing tendencies.

Conclusions A transversely excited multi-atmospheric-pressure CO₂ laser is studied. A gas mixture ($V_{\text{CO}_2} : V_{\text{N}_2} : V_{\text{He}} = 2 : 1 : 16$) at 7 atm was adopted in the cavity. The discharging voltage was 72 kV and the total injection energy was 19.88 J. The resonant cavity contained a Ge coupling window with the reflective index of 36% and a diffraction grating with the grating constant of 1/150 mm driven by a servo motor. The total tuning range of CO₂ laser in the 9.2–10.8 μm band is about 1.43 μm with four bands (9R, 9P, 10R, 10P). New records were achieved at line 10P(20) (10.59 μm) with the corresponding maximum energy of 590 mJ and the minimum pulse width of 35.7 ns. The estimated pulse peak

power was about 16 MW. Obvious continuously tunable properties were measured from line 10R(32) to line 10R(26). In the future, output properties under higher working pressures will be studied and the coupling efficiency will be optimized. In combination with the study of multi-atmospheric-pressure CO₂ laser amplifier, an oscillator-amplifier system is in the plan, which may be helpful to the research progress of laser isotope separation.

Key words lasers; CO₂ laser; multiple atmospheric pressures; continuous tuning; pulse width compression